
Unlocking Feature Visualization for Deeper Networks with MAGNITUDE Constrained Optimization

Thomas Fel^{*1,2,4}, Thibaut Boissin^{*2,3}, Victor Boutin^{*1,2}, Agustín Picard^{*2,3}, Paul Novello^{*2,3},
Julien Colin^{1,5}, Drew Linsley¹, Tom Rousseau⁴, Rémi Cadène¹, Laurent Gardes⁴,
Thomas Serre^{1,2}

¹Carney Institute for Brain Science, Brown University

²Artificial and Natural Intelligence Toulouse Institute

³Institut de Recherche Technologique Saint-Exupéry

⁴Innovation & Research Division, SNCF

⁵ELLIS Alicante, Spain.

{thomas_fel@brown.edu, thibaut.boissin@irt-saintexupery.com}

Abstract

Feature visualization has gained substantial popularity, particularly after the influential work by Olah et al. in 2017, which established it as a crucial tool for explainability. However, its widespread adoption has been limited due to a reliance on tricks to generate interpretable images, and corresponding challenges in scaling it to deeper neural networks. Here, we describe **MACO**, a simple approach to address these shortcomings. The main idea is to generate images by optimizing the phase spectrum while keeping the magnitude constant to ensure that generated explanations lie in the space of natural images. Our approach yields significantly better results – both qualitatively and quantitatively – and unlocks efficient and interpretable feature visualizations for large state-of-the-art neural networks. We also show that our approach exhibits an attribution mechanism allowing us to augment feature visualizations with spatial importance. We validate our method on a novel benchmark for comparing feature visualization methods, and release its visualizations for all classes of the ImageNet dataset on <https://serre-lab.github.io/Lens/>.

Overall, our approach unlocks, for the first time, feature visualizations for large, state-of-the-art deep neural networks without resorting to any parametric prior image model.

1 Introduction

The field of Explainable Artificial Intelligence (XAI) [2, 3] has largely focused on characterizing computer vision models through the use of attribution methods [4–13]. These methods aim to explain the decision strategy of a network by assigning an importance score to each input pixel (or group of input pixels [14–16]), according to their contribution to the overall decision. Such approaches only offer a partial understanding of the learned decision processes as they aim to identify the location of the most discriminative features in an image, the “where”, leaving open the “what” question, *i.e.* the semantic meaning of those features. Recent work [17–22] has highlighted the intrinsic limitations of attribution methods [23–26], calling for the development of methods that provide a complementary explanation regarding the “what”.

Feature visualizations provide a bridge to fill this gap via the generation of images that elicit a strong response from specifically targeted neurons (or groups of neurons). One of the simplest approaches uses gradient ascent to search for such an image. In the absence of regularization, this optimization is

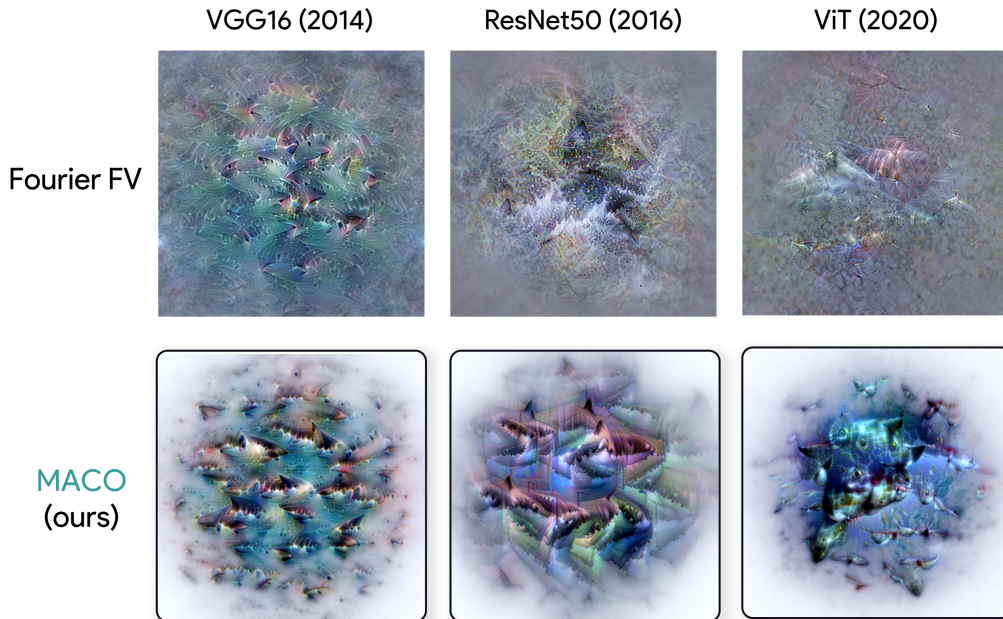


Figure 1: **Comparison between feature visualization methods for “White Shark” classification. (Top)** Standard Fourier preconditioning-based method for feature visualization [1]. **(Bottom)** Proposed approach, **MACO**, which incorporates a Fourier spectrum magnitude constraint.

known to yield highly noisy images – sometimes considered adversarial [27]. Hence, regularization methods are essential to rendering more acceptable candidate images. Such regularizations can consist of penalizing high frequencies in the Fourier domain [1, 28–31], regularizing the optimization process with data augmentation [1, 32–35] or restricting the search space to a subspace parameterized by a generative model [36–39]. The first two approaches provide faithful visualizations, as they only depend on the model under study; unfortunately, in practice, they still fail on large modern classification models (*e.g.*, ResNet50V2 [40] and ViT [41], see Figure 1). The third approach yields interpretable feature visualizations even for large models but at the cost of major biases: in that case, it is impossible to disentangle the true contributions of the model under study from those of the generative prior model. Herein, we introduce a new feature visualization approach that is applicable to the largest state-of-the-art networks without relying on any parametric prior image model.

Our proposed approach, called **M**agnitude **C**onstrained **O**ptimization (**MACO**), builds on the seminal work by Olah *et al.* who described the first method to optimize for maximally activating images in the Fourier space in order to penalize high-frequency content [1]. **MACO** also uses this phase/magnitude decomposition of the Fourier spectrum, but it solely optimizes the image phase while keeping its magnitude constant. Such a constraint is motivated by psychophysics experiments that have shown that humans are more sensitive to differences in phase than in magnitude [42–46]. Our contributions with **MACO** are threefold:

- (i) We unlock feature visualizations for large modern CNNs without resorting to any strong parametric image prior (see Figure 1).
- (ii) We describe how to leverage the gradients obtained throughout **MACO**’s optimization process to combine feature visualization with attribution methods, thereby explaining both “what” activates a neuron and “where” it is located in an image.
- (iii) We introduce new metrics to compare the feature visualizations produced with **MACO** to those generated with other methods.

As an application of our approach, we use **MACO** to produce feature visualizations for FlexViT [47] and ViT [41] (logits and intermediate layers; see Figure 4). We also employ **MACO** on a feature inversion task to generate images that yield the same activations as target images to better understand what information is getting propagated through the network and which parts of the image are getting discarded by the model (on ViT, see Figure 5). Finally, we show how to combine **MACO** with a state-of-the-art concept-based explainability method [48] (see Figure 6). Much like

feature visualization, this method produces explanations on the semantic “what” that drives a model’s prediction by decomposing the latent space of the neural network into a series of “directions” – denoted concepts. More importantly, it also provides a way to locate each concept in the input image under study, thus unifying both axes – “what” and “where”. As feature visualization can be used to optimize in directions in the network’s representation space, we employ **MACO** to generate concept visualizations, thus allowing us to improve the human interpretability of concepts and reducing the risk of confirmation bias. We showcase these concept visualizations on an interactive website, which will be released upon acceptance. The website allows browsing the most important concepts learned by a ResNet50 for all 1,000 classes of ImageNet [40].

2 Related Work

Feature visualization methods involve solving an optimization problem to find an input image that maximizes the activation of a target element (neuron, layer, or whole model) [10]. Most of the approaches developed in the field fall along a spectrum based on how strongly they regularize the model. At one end of the spectrum, if no regularization is used, the optimization process can search the whole image space, but this tends to produce noisy images and nonsensical high-frequency patterns [49].

To circumvent this issue, researchers have proposed to penalize high-frequency in the resulting images – either by reducing the variance between neighboring pixels [28], by imposing constraints on the image’s total variation [38, 39, 4], or by blurring the image at each optimization step [29]. However, in addition to rendering images of debatable validity, these approaches also suppress genuine, interesting high-frequency features, including edges. To mitigate this issue, a bilateral filter may be used instead of blurring, as it has been shown to preserve edges and improve the overall result [30]. Other studies have described a similar technique to decrease high frequencies by operating directly on the gradient, with the goal of preventing their accumulation in the resulting visualization [31]. One advantage of reducing high frequencies present in the gradient, as opposed to the visualization itself, is that it prevents high frequencies from being amplified by the optimizer while still allowing them to appear in the final image if consistently encouraged by the gradient. This process, known as “preconditioning” in optimization, can greatly simplify the optimization problem. The Fourier transform has been shown to be a successful preconditioner as it forces the optimization to be performed in a decorrelated and whitened image space [1]. The feature visualization technique we introduce in this work leverages a similar preconditioning. The emergence of high-frequency patterns in the absence of regularization is associated with a lack of robustness and sensitivity of the neural network to adversarial examples [27], and consequently, these patterns are less often observed in adversarially robust models [34, 33, 32]. An alternative strategy to promote robustness involves enforcing small perturbations, such as jittering, rotating, or scaling, in the visualization process [35], which, when combined with a frequency penalty [1], has been proved to greatly enhance the generated images.

Unfortunately, previous methods in the field of feature visualization have been limited in their ability to generate visualizations for newer architectures beyond VGG, resulting in a lack of interpretable visualizations for larger networks like ResNets [1]. Consequently, researchers have shifted their focus to approaches that leverage statistically learned priors to produce highly realistic visualizations. One such approach involves training a generator, like a GAN [38] or an autoencoder [50, 39], to map points from a latent space to realistic examples and optimizing within that space. Alternatively, a prior can be learned to provide the gradient (w.r.t the input) of the probability and optimize both the prior and the objective jointly [39, 30]. Another method involves approximating a generative model prior by penalizing the distance between output patches and the nearest patches retrieved from a database of image patches collected from the training data [36]. Although it is well-established that learning an image prior produces realistic visualizations, it is difficult to distinguish between the contributions of the generative models and that of the neural network under study. Hence, in this work, we focus on the development of visualization methods that rely on minimal priors to yield the least biased visualizations.

3 Magnitude-Constrained Feature Visualization

Notations Without loss of generality, we consider a standard supervised image classification problem. We assume we have access to a pretrained classifier f , trained on an image dataset $(x_n)_{n \in [1, N]}$ which contains N samples drawn from a probability distribution of natural images

\mathcal{D} : $\forall n \in \llbracket 1, N \rrbracket$, $\mathbf{x}_n \sim \mathcal{D}$. \mathbf{f} maps real-valued images \mathbf{x} from an input space $\mathcal{X} \subseteq \mathbb{R}^{W \times H}$ to K -dimensional labels \mathbf{y} (lying in an output space $\mathcal{Y} \subseteq \mathbb{R}^K$). We respectively denote \mathcal{F} and \mathcal{F}^{-1} the Discrete Fourier Transform (DFT) on $\mathbb{R}^{W \times H}$ and its inverse. Therefore: $\forall \mathbf{x} \in \mathbb{R}^{W \times H}$, $\mathcal{F}(\mathbf{x}) \in \mathbb{C}^{W \times H}$ and $(\mathcal{F} \circ \mathcal{F}^{-1})(\mathbf{x}) = \mathbf{x}$. We use the training samples to estimate the expected magnitude spectrum $\mathbb{E}_{\mathbf{x} \sim \mathcal{D}}(|\mathcal{F}(\mathbf{x})|)$, using the empirical mean. We assume the classifier \mathbf{f} is a CNN containing I layers $(L_i)_{i \in \llbracket 1, I \rrbracket}$, and i^{th} layer L_i includes J neurons $(L_{i,j})_{j \in \llbracket 1, J \rrbracket}$. We define \mathcal{A} the set of neurons that we want to explain, with $\mathcal{A} = \{(i_1, j_1), \dots, (i_k, j_k)\}$, which could be all the neurons in a channel, a single logit, or an entire layer. Finally, we denote by $\mathcal{L}_{\mathcal{A}}$ the loss associated with these neurons that seek to maximize their activations.

Optimization Criterion. The primary goal of a feature visualization method is to produce an image \mathbf{x}^* that maximizes a given criterion $\mathcal{L}_{\mathcal{A}}(\mathbf{x}) \in \mathbb{R}$; usually some value aggregated over a subset of weights in a neural network \mathbf{f} (neurons, channels, layers, logits). A concrete example consists in finding a natural "prototypical" image \mathbf{x}^* of a class $k \in \llbracket 1, K \rrbracket$ without using a dataset or generative models. However, optimizing in the pixel space $\mathbb{R}^{W \times H}$ is known to produce noisy, adversarial-like \mathbf{x}^* (see section 2). Therefore, the optimization is constrained using a regularizer $\mathcal{R} : \mathcal{X} \rightarrow \mathbb{R}^+$ to penalize unrealistic images:

$$\mathbf{x}^* = \arg \max_{\mathbf{x} \in \mathcal{X}} \mathcal{L}_{\mathcal{A}}(\mathbf{x}) - \lambda \mathcal{R}(\mathbf{x}). \quad (1)$$

In Eq. 1, λ is a hyperparameter used to balance the main optimization criterion $\mathcal{L}_{\mathcal{A}}$ and the regularizer \mathcal{R} . Finding a regularizer that perfectly matches the structure of natural images is hard, so proxies have to be used instead. Previous studies have explored various forms of regularization spanning from total variation, ℓ_1 , or ℓ_2 loss [38, 39, 4]. More successful attempts rely on the reparametrization of the optimization problem in the Fourier domain rather than on regularization.

3.1 A Fourier perspective

Mordvintsev *et al.* [51] noted in their seminal work that one could use differentiable image parametrizations to facilitate the maximization of $\mathcal{L}_{\mathcal{A}}$. Olah *et al.* [1] proposed to re-parametrize the images using their Fourier spectrum. Such a parametrization allows amplifying the low frequencies using a scalar \mathbf{w} . Formally, the prototypical image \mathbf{x}^* can be written as $\mathbf{x}^* = \mathcal{F}^{-1}(\mathbf{z}^* \odot \mathbf{w})$ with $\mathbf{z}^* = \arg \max_{\mathbf{z} \in \mathbb{C}^{W \times H}} \mathcal{L}_{\mathcal{A}}(\mathcal{F}^{-1}(\mathbf{z} \odot \mathbf{w}))$. Finding \mathbf{x}^* boils down to optimizing a Fourier buffer $\mathbf{z} = \mathbf{a} + i\mathbf{b}$ together with boosting the low-frequency components and then recovering the final image by inverting the optimized Fourier buffer using inverse Fourier transform.

However, multiple studies have shown that the resulting images are not sufficiently robust, in the sense that a small change in the image can cause the criterion $\mathcal{L}_{\mathcal{A}}$ to drop. Therefore, it is common to see robustness transformations applied to candidate images throughout the optimization process. In other words, the goal is to ensure that the generated image satisfies the criterion even if it is rotated by a few degrees or jittered by a few pixels. Formally, given a set of possible transformation functions – sometimes called augmentations – that we denote \mathcal{T} such that for any transformation $\tau \sim \mathcal{T}$, we have $\tau(\mathbf{x}) \in \mathcal{X}$, the optimization becomes $\mathbf{z}^* = \arg \max_{\mathbf{z} \in \mathbb{C}^{W \times H}} \mathbb{E}_{\tau \sim \mathcal{T}}(\mathcal{L}_{\mathcal{A}}((\tau \circ \mathcal{F}^{-1})(\mathbf{z} \odot \mathbf{w}))$.

Empirically, it is common knowledge that the deeper the models are, the more transformations are needed and the greater their magnitudes should be. To make their approach work on models like VGG, Olah *et al.* [1] used no less than a dozen transformations. However, this method fails for modern architectures, no matter how many transformations are applied. We argue that this may come from the low-frequency scalar (or booster) no longer working with models that are too deep. For such models, high frequencies eventually come through, polluting the resulting images with high-frequency content – making them impossible to interpret by humans. To empirically illustrate this phenomenon, we compute the k logit visualizations obtained by maximizing each of the logits corresponding to

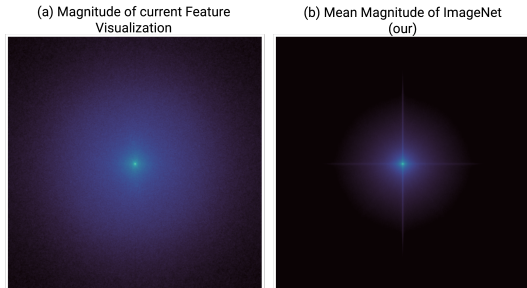


Figure 2: **High-frequency leakage.** Comparison between the mean power spectra of visualizations generated using (a) the technique by Olah *et al.* [1] on a ViT and (b) our constrained magnitude. The heat maps are on the same scale. The amount of mid- and high-frequencies in (a) is a plausible reason for why their visualizations do not look as realistic as ours.

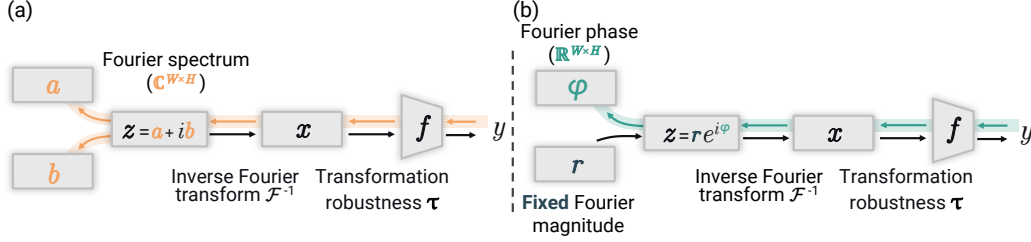


Figure 3: **Overview of the approach:** (a) Current Fourier parameterization approaches optimize the entire spectrum (yellow arrow). (b) In contrast, the optimization flow in our approach (green arrows) goes from the network activation (y) to the phase of the spectrum (φ) of the input image (x).

the k classes of a ViT using the parameterization used by Olah *et al.* In Figure 2 (left), we show the average of the spectrum of these generated visualizations over all classes: $\frac{1}{k} \sum_{i=1}^k |\mathcal{F}(\mathbf{x}_i^*)|$. We compare it with the average spectrum of images on the ImageNet dataset (denoted \mathcal{D}): $\mathbb{E}_{\mathbf{x} \sim \mathcal{D}}(|\mathcal{F}(\mathbf{x})|)$ (Figure 2, right panel). We observe that the images obtained through optimization put much more energy into high frequencies compared to natural images. Note that we did not observe this phenomenon in older models such as LeNet or VGG.

In the following section, we introduce our method named **MACO**, which is motivated by this observation. We constrain the magnitude of the visualization to a natural value, enabling natural visualization for any contemporary model, and reducing the number of required transformations to only two.

3.2 MACO: from Regularization to Constraint

Parameterizing the image in the Fourier space makes it possible to directly manipulate the image in the frequency domain. We propose to take a step further and decompose the Fourier spectrum z into its polar form $z = r e^{i\varphi}$ instead of its cartesian form $z = a + ib$, which allows us to disentangle the magnitude (r) and the phase (φ).

It is known that human recognition of objects in images is driven not by magnitude but by phase [42–46]. Motivated by this, we propose to optimize the phase of the Fourier spectrum while fixing its magnitude to a typical value of a natural image (with few high frequencies). In particular, the magnitude is kept constant at the average magnitude computed over a set of natural images (such as ImageNet), so $r = \mathbb{E}_{\mathbf{x} \sim \mathcal{D}}(|\mathcal{F}(\mathbf{x})|)$. Note that this spectrum needs to be calculated only once and can be used at will for other tasks.

Therefore, our method does not backpropagate through the entire Fourier spectrum but only through the phase (Figure 3), thus reducing the number of parameters to optimize by half. Since the magnitude of our spectrum is constrained, we no longer need hyperparameters such as λ or scaling factors, and the generated image at each step is naturally plausible in the frequency domain. We also enhance the quality of our visualizations via two data augmentations: random crop and additive uniform noise. To the best of our knowledge, our approach is the first to completely alleviate the need for explicit regularization – using instead a hard constraint on the solution of the optimization problem for feature visualization. To summarize, we formally introduce **MACO**:

Definition 3.1 (MACO). *The feature visualization results from optimizing the parameter vector φ such that:*

$$\varphi^* = \arg \max_{\varphi \in \mathbb{R}^{W \times H}} \mathbb{E}_{\tau \sim \mathcal{T}} (\mathcal{L}_{\mathcal{A}}((\tau \circ \mathcal{F}^{-1})(r e^{i\varphi}))) \quad \text{s.t.} \quad r = \mathbb{E}_{\mathbf{x} \sim \mathcal{D}}(|\mathcal{F}(\mathbf{x})|)$$

The feature visualization is then obtained by applying the inverse Fourier transform to the optimal complex-valued spectrum: $\mathbf{x}^* = \mathcal{F}^{-1}(r e^{i\varphi^*})$

Algorithm 1 MACO

Require: $r, \varphi_0 \sim \mathcal{U}([-\pi, \pi])^{W \times H}$

Require: $\alpha = 0$

for $n \in \llbracket 0, N \rrbracket$ **do**

$\tau = \text{sample}(\mathcal{T})$

$\mathbf{x}_n = (\tau \circ \mathcal{F}^{-1})(r e^{i\varphi_n})$

$\varphi_{n+1} = \varphi_n + \eta \nabla_{\varphi} \mathcal{L}_{\mathcal{A}}(\mathbf{x}_n)$

$\alpha = \alpha + |\nabla_{\mathbf{x}_n} \mathcal{L}_{\mathcal{A}}(\mathbf{x}_n)|$

end for

return $\mathbf{x}^* = \mathcal{F}^{-1}(r e^{i\varphi_N}), \alpha$

Transparency for free Visualizations often suffer from repeated patterns or unimportant elements in the generated images. This can lead to readability problems or confirmation biases [52]. It is important to ensure that the user is looking at what is truly important in the feature visualization. The concept of transparency, introduced in [51], addresses this issue but induces additional implementation efforts and computational costs.

We propose an effective approach, which leverages attribution methods, that yields a transparency map α for the associated feature visualization without any additional cost. Our solution shares theoretical similarities with SmoothGrad [5] and takes advantage of the fact that during backpropagation, we can obtain the intermediate gradients on the input $\partial\mathcal{L}_A(\mathbf{x})/\partial\mathbf{x}$ for free as $\frac{\partial\mathcal{L}_A(\mathbf{x})}{\partial\varphi} = \frac{\partial\mathcal{L}_A(\mathbf{x})}{\partial\mathbf{x}} \frac{\partial\mathbf{x}}{\partial\varphi}$. We store these gradients throughout the optimization process and then average them, as done in SmoothGrad, to identify the areas that have been modified/attended to by the model the most during the optimization process. We note that a similar technique has recently been used to explain diffusion models [53]. In Algorithm 1, we provide pseudo-code for **MACO** and an example of the transparency maps in Figure 5 (third column).

4 Evaluation

We now describe and compute three different scores to compare the different feature visualization methods: Fourier (Olah *et al.*), CBR (optimization in the pixel space), and **MACO** (ours). It is important to note that these scores are only applicable to output logit visualizations. Also, note that we restrict the benchmark to methods that do not rely on any learned image priors. Indeed, these priors parametrize a manifold where all the images are likely to have high plausibility and FID score, so will feature visualization. Hence, the benchmark might not be adapted to such methods (see supplementary materials section ?? for an expanded discussion on limitations).

Plausibility score. We consider a feature visualization plausible when it is similar to the distribution of images belonging to the class it represents. We quantify the plausibility through an OOD metric (Deep-KNN, recently used in [54]): it measures how far a feature visualization deviates from the corresponding ImageNet object category images based on their representation in the network’s intermediate layers (see Table 1).

FID score. The FID quantifies the similarity between the distribution of the feature visualizations and that of natural images for the same object category. Importantly, the FID measures the distance between two distributions, while the plausibility score quantifies the distance from a sample to a distribution. To compute the FID, we used images from the ImageNet validation set and used the Inception v3 last layer (see Table 1). Additionally, we center-cropped our 512×512 images to 299×299 images to avoid the center-bias problem [37].

Transferability score. This score measures how consistent the feature visualizations are with other pre-trained classifiers. To compute the transferability score, we feed the obtained feature visualizations into 6 additional pre-trained classifiers (MobileNet [55], VGG16 [56], Xception [57], EfficientNet [58], Tiny ConvNext [59] and Densenet [60]), and we report their classification accuracy (see Table 2).

All scores are computed using 500 feature visualizations, each of them maximizing the logit of one of the ImageNet classes obtained on the FlexiViT [47], ViT[61], and ResNetV2[62] models. For the feature visualizations derived from Olah *et al.* [1], we used all 10 transformations set from the Lucid library*. CBR denotes an optimization in pixel space and using the same 10 transformations, as described in [29]. For **MACO**, τ only consists of two transformations; first we add uniform noise $\delta \sim \mathcal{U}([-0.1, 0.1])^{W \times H}$ and crops and resized the image with a crop size drawn from the normal distribution $\mathcal{N}(0.25, 0.1)$, which corresponds on average to 25% of the image. We used the NAdam optimizer [63] with a $lr = 1.0$ and $N = 256$ optimization steps. Finally, we used the implementation of [1] and CBR which are available in the Xplique library [64] † which is based on Lucid.

For all tested metrics, we observe that **MACO** produces better feature visualizations than those generated by Olah *et al.* [1] and CBR [29]. We would like to emphasize that our proposed evaluation scores represent the first attempt to provide a systematic evaluation of feature visualization methods,

*<https://github.com/tensorflow/lucid>

†<https://github.com/deel-ai/xplique>

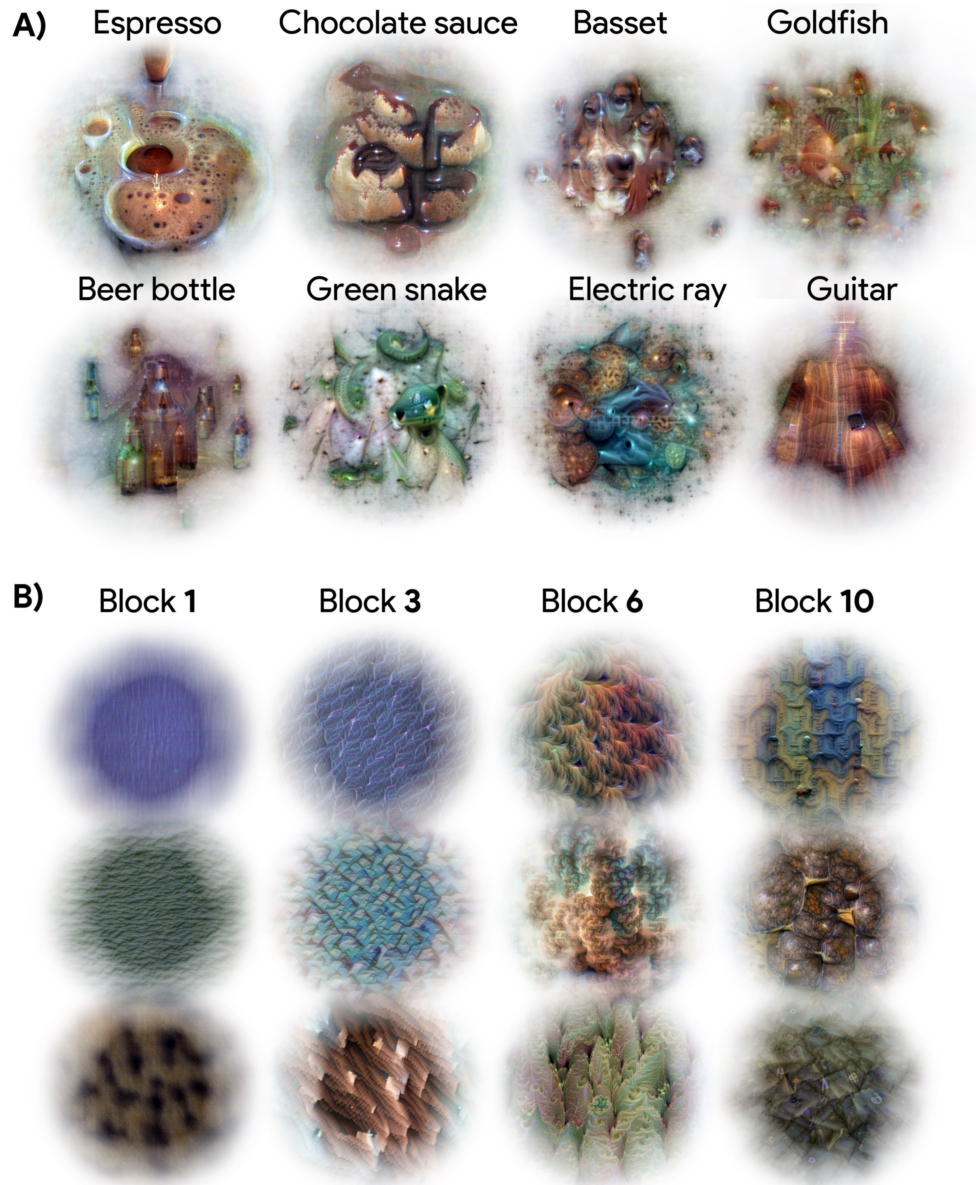


Figure 4: (A) **Logits** and (B) **internal representations** of FlexiViT. **MACO** was used to maximize the activations of (A) logit units and (B) specific channels located in different blocks of the FlexViT (blocks 1, 2, 6 and 10 from left to right).

but we acknowledge that each individual metric on its own is insufficient and cannot provide a comprehensive assessment of a method’s performance (see section ??). However, when taken together, the three proposed scores provide a more complete and accurate evaluation of the feature visualization methods.

5 Applications

We demonstrate the versatility of the proposed **MACO** technique by applying it to three different XAI applications:

	FlexiViT	ViT	ResNetV2		FlexiViT	ViT	ResNetV2
• Plausibility score (1-KNN) (\downarrow)				• Transferability score (\uparrow): MACO / Fourier [1]			
MACO	1473	1097	1248	MobileNet	68 / 38	48 / 37	93 / 36
Fourier [1]	1815	1817	1837	VGG16	64 / 30	50 / 30	90 / 20
CBR [29]	1866	1920	1933	Xception	85 / 61	73 / 62	97 / 64
• FID Score (\downarrow)				Eff. Net	88 / 25	63 / 25	82 / 21
MACO	230.68	241.68	312.66	ConvNext	96 / 52	84 / 55	93 / 60
Fourier [1]	250.25	257.81	318.15	DenseNet	84 / 32	66 / 31	93 / 25
CBR [29]	247.12	268.59	346.41				

Table 1: Plausibility and FID scores for different feature visualization methods applied on FlexiViT, ViT and ResNetV2

Table 2: Transferability scores for different feature visualization methods applied on FlexiViT, ViT and ResNetV2.

Logit and internal state visualization. For logit visualization, the optimization objective is to maximize the activation of a specific unit in the logits vector of a pre-trained neural network (here a FlexiViT[47]). The resulting visualizations provide insights into the features that contribute the most to a class prediction (refer to Figure 4a). For internal state visualization, the optimization objective is to maximize the activation of specific channels located in various intermediate blocks of the network (refer to Figure 4b). This visualization allows us to better understand the kind of features these blocks – of a FlexiViT[47] in the figure – are sensitive to.

Feature inversion. The goal of this application is to find an image that produces an activation pattern similar to that of a reference image. By maximizing the similarity to reference activations, we are able to generate images representing the same semantic information at the target layer but without the parts of the original image that were discarded in the previous stages of the network, which allows us to better understand how the model operates. Figure 5 displays the images (second column) that match the activation pattern of the penultimate layer of a ViT when given the images from the first column. We also provide examples of transparency masks based on attribution (third column), which we apply to the feature visualizations to enhance them (fourth column).

Concept visualization. Herein we combine **MACO** with concept-based explainability. Such methods aim to increase the interpretability of activation patterns by decomposing them into a set of concepts [65]. In this work, we leverage the CRAFT concept-based explainability method [48], which uses Non-negative Matrix Factorization to decompose activation patterns into main directions – that are called concepts –, and then, we apply **MACO** to visualize these concepts in the pixel space. To do so, we optimize the visualization such that it matches the concept activation patterns. In Figure 6, we present the top 3 most important concepts (one concept per column) for five different object categories (one category per row) in a ResNet50 trained on ImageNet. The concepts’ visualizations are followed by a mosaic of patches extracted from natural images: the patches that maximally activate the corresponding concept.

6 Limitations

We have demonstrated the generation of realistic explanations for large neural networks by imposing constraints on the magnitude of the spectrum. However, it is important to note that generating realistic images does not necessarily imply effective explanation of the neural networks. The metrics introduced in this paper allow us to claim that our generated images are closer to natural images in latent space, that our feature visualizations are more plausible and better reflect the original distribution. However, they do not necessarily indicate that these visualizations aid humans in effectively communicating with the models or conveying information easily to humans. Furthermore, in order for a feature visualization to provide informative insights about the model, including spurious features, it may need to generate visualizations that deviate from the spectrum of natural images. Consequently, these visualizations might yield lower scores using our proposed metrics. Simultaneously, several interesting studies have highlighted the weaknesses and limitations of feature visualizations [52, 66, 67]. One prominent criticism is their lack of interpretability for humans, with research demonstrating that dataset examples are more useful than feature visualizations in

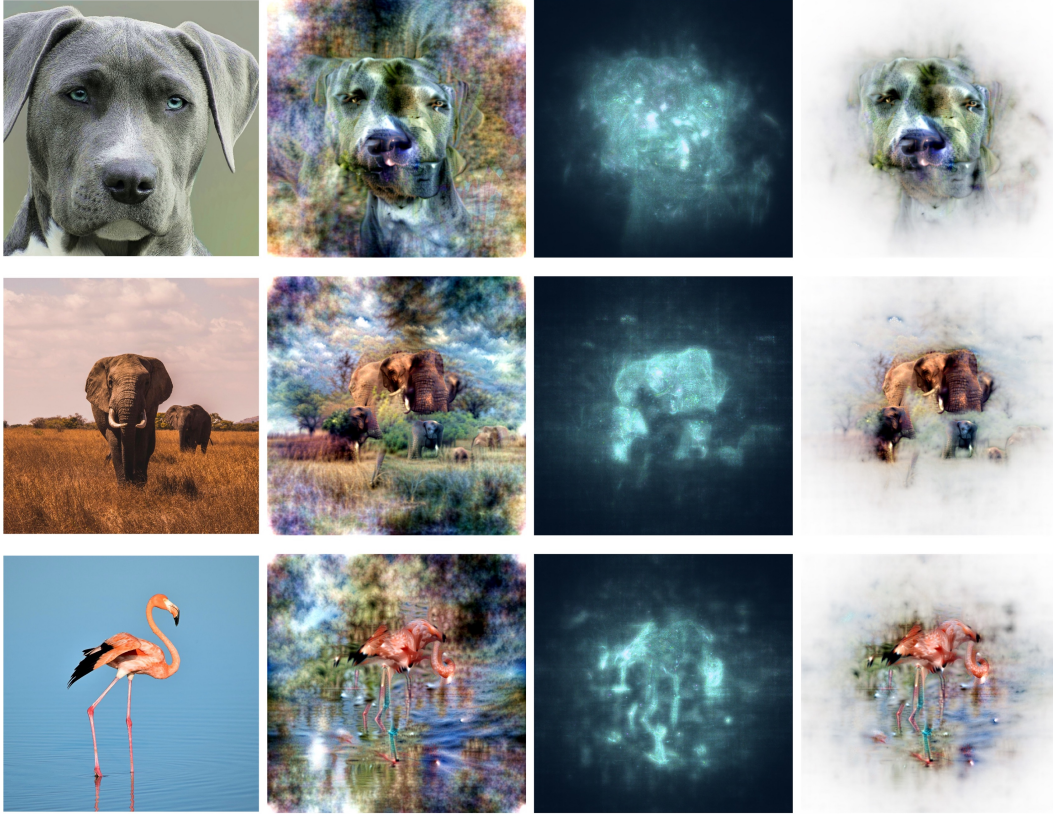


Figure 5: **Feature inversion and transparency mask.** Images in the second column match the activation pattern of the penultimate layer of a ViT when fed with the images of the first column. In the third column, we show their corresponding attribution-based transparency masks, leading to better feature visualization when applied (fourth column).

understanding convolutional neural networks (CNNs) [52]. This can be attributed to the lack of realism in feature visualizations and their isolated use as an explainability technique. With our approach, **MACO**, we take an initial step towards addressing this limitation by introducing magnitude constraints, which lead to qualitative and quantitative improvements. Additionally, through our website, we promote the use of feature visualizations as a supportive and complementary tool alongside other methods such as concept-based explainability, exemplified by CRAFT [48]. We emphasize the importance of feature visualizations in combating confirmation bias and encourage their integration within a comprehensive explainability framework.

7 Conclusions

In this paper, we introduced a novel approach, **MACO**, for efficiently generating feature visualizations in modern deep neural networks based on (i) a hard constraint on the magnitude of the spectrum to ensure that the generated visualizations lie in the space of natural images, and (ii) a new attribution-based transparency mask to augment these feature visualizations with the notion of spatial importance. This enhancement allowed us to scale up and unlock feature visualizations on large modern CNNs and vision transformers without the need for strong – and possibly misleading – parametric priors. We also complement our method with a set of three metrics to assess the quality of the visualizations. Combining their insights offers a way to compare the techniques developed in this branch of XAI more objectively. We illustrated the scalability of **MACO** with feature visualizations of large models like ViT, but also feature inversion and concept visualization. Lastly, by improving the realism of the generated images without using an auxiliary generative model, we supply the field of XAI with a reliable tool for explaining the semantic (“what” information) of modern vision models.

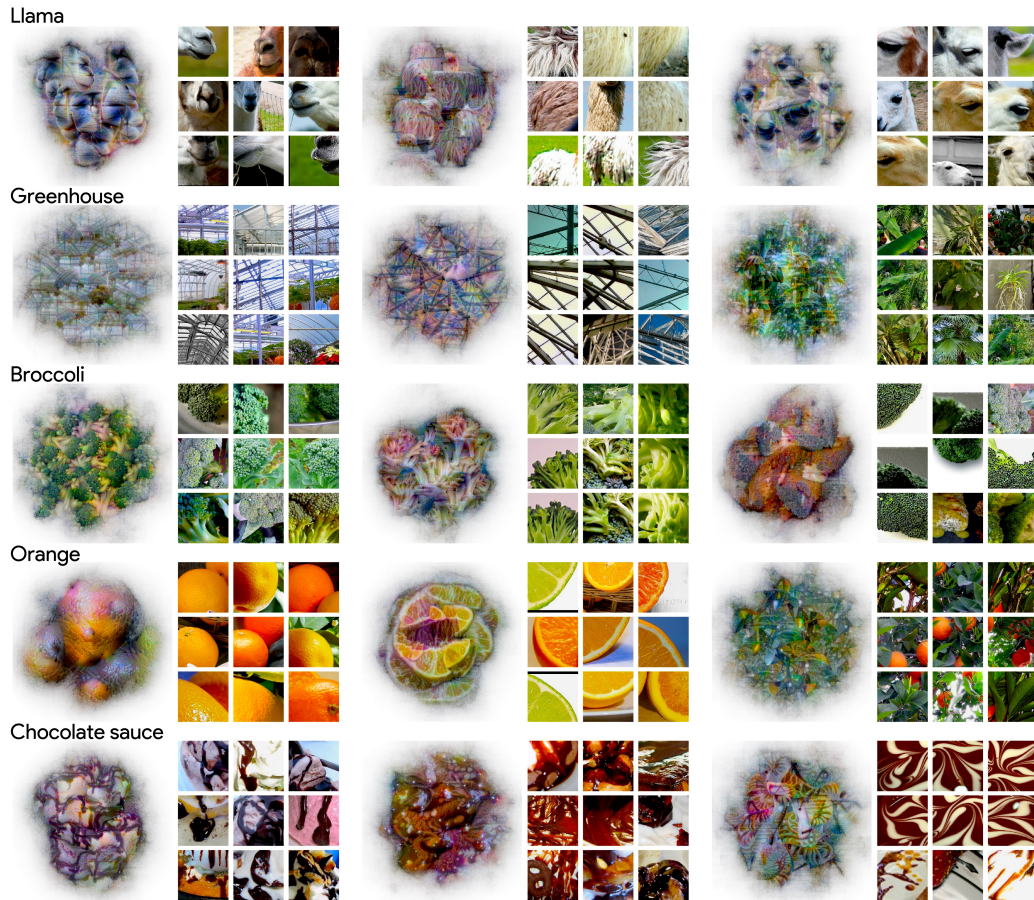


Figure 6: **Combining MACO with CRAFT [48] to visualize concepts.** We leverage CRAFT to identify significant concepts within a class – like a llama’s mouth, fur, and eyes – and propose to combine these concepts with their corresponding feature visualizations that maximize the concept vector. The concepts are extracted from a ResNet50 trained on ImageNet. All visualizations for all ImageNet classes will be available at [Lens](#).

References

- [1] Chris Olah, Alexander Mordvintsev, and Ludwig Schubert. Feature visualization. *Distill*, 2(11):e7, 2017.
- [2] Finale Doshi-Velez and Been Kim. Towards a rigorous science of interpretable machine learning. *ArXiv e-print*, 2017.
- [3] Alon Jacovi, Ana Marasović, Tim Miller, and Yoav Goldberg. Formalizing trust in artificial intelligence: Prerequisites, causes and goals of human trust in ai. In *Proceedings of the 2021 ACM conference on fairness, accountability, and transparency*, pages 624–635, 2021.
- [4] Karen Simonyan, Andrea Vedaldi, and Andrew Zisserman. Deep inside convolutional networks: Visualising image classification models and saliency maps. In *Workshop Proceedings of the International Conference on Learning Representations (ICLR)*, 2014.
- [5] Daniel Smilkov, Nikhil Thorat, Been Kim, Fernanda Viégas, and Martin Wattenberg. Smoothgrad: removing noise by adding noise. In *Workshop on Visualization for Deep Learning, Proceedings of the International Conference on Machine Learning (ICML)*, 2017.
- [6] Ramprasaath R Selvaraju, Michael Cogswell, Abhishek Das, Ramakrishna Vedantam, Devi Parikh, and Dhruv Batra. Grad-cam: Visual explanations from deep networks via gradient-based localization. In *Proceedings of the IEEE international conference on computer vision*, pages 618–626, 2017.
- [7] Thomas Fel, Remi Cadene, Mathieu Chalvidal, Matthieu Cord, David Vigouroux, and Thomas Serre. Look at the variance! efficient black-box explanations with sobol-based sensitivity analysis. In *Advances in Neural Information Processing Systems (NeurIPS)*, 2021.
- [8] Paul Novello, Thomas Fel, and David Vigouroux. Making sense of dependence: Efficient black-box explanations using dependence measure. In *Advances in Neural Information Processing Systems (NeurIPS)*, 2022.
- [9] Mukund Sundararajan, Ankur Taly, and Qiqi Yan. Axiomatic attribution for deep networks. In *Proceedings of the International Conference on Machine Learning (ICML)*, 2017.
- [10] Matthew D Zeiler and Rob Fergus. Visualizing and understanding convolutional networks. In *Computer Vision—ECCV 2014: 13th European Conference, Zurich, Switzerland, September 6–12, 2014, Proceedings, Part I 13*, pages 818–833. Springer, 2014.
- [11] Avanti Shrikumar, Peyton Greenside, and Anshul Kundaje. Learning important features through propagating activation differences. In *Proceedings of the International Conference on Machine Learning (ICML)*, 2017.
- [12] Ruth C. Fong and Andrea Vedaldi. Interpretable explanations of black boxes by meaningful perturbation. In *Proceedings of the IEEE International Conference on Computer Vision (ICCV)*, 2017.
- [13] Mara Graziani, Iam Palatnik de Sousa, Marley MBR Vellasco, Eduardo Costa da Silva, Henning Müller, and Vincent Andrearczyk. Sharpening local interpretable model-agnostic explanations for histopathology: improved understandability and reliability. In *Medical Image Computing and Computer Assisted Intervention (MICCAI)*. Springer, 2021.
- [14] Vitali Petsiuk, Abir Das, and Kate Saenko. Rise: Randomized input sampling for explanation of black-box models. In *Proceedings of the British Machine Vision Conference (BMVC)*, 2018.
- [15] Thomas Fel, Melanie Ducoffe, David Vigouroux, Remi Cadene, Mikael Capelle, Claire Nicodeme, and Thomas Serre. Don’t lie to me! robust and efficient explainability with verified perturbation analysis. *Proceedings of the IEEE Conference on Computer Vision and Pattern Recognition (CVPR)*, 2023.
- [16] Marouane El Idrissi, Nicolas Bousquet, Fabrice Gamboa, Bertrand Iooss, and Jean-Michel Loubes. On the coalitional decomposition of parameters of interest, 2023.
- [17] Julien Colin, Thomas Fel, Rémi Cadène, and Thomas Serre. What i cannot predict, i do not understand: A human-centered evaluation framework for explainability methods. *Advances in Neural Information Processing Systems (NeurIPS)*, 2021.
- [18] Sunnie S. Y. Kim, Nicole Meister, Vikram V. Ramaswamy, Ruth Fong, and Olga Russakovsky. HIVE: Evaluating the human interpretability of visual explanations. In *Proceedings of the IEEE European Conference on Computer Vision (ECCV)*, 2022.
- [19] Giang Nguyen, Daeyoung Kim, and Anh Nguyen. The effectiveness of feature attribution methods and its correlation with automatic evaluation scores. *Advances in Neural Information Processing Systems (NeurIPS)*, 2021.
- [20] Anh Nguyen, Jason Yosinski, and Jeff Clune. Understanding neural networks via feature visualization: A survey. *Explainable AI: interpreting, explaining and visualizing deep learning*, pages 55–76, 2019.
- [21] Leon Sixt, Martin Schuessler, Oana-Iuliana Popescu, Philipp Weiß, and Tim Landgraf. Do users benefit from interpretable vision? a user study, baseline, and dataset. *Proceedings of the International Conference on Learning Representations (ICLR)*, 2022.

- [22] Peter Hase and Mohit Bansal. Evaluating explainable ai: Which algorithmic explanations help users predict model behavior? *Proceedings of the Annual Meeting of the Association for Computational Linguistics (ACL Short Papers)*, 2020.
- [23] Leon Sixt, Maximilian Granz, and Tim Landgraf. When explanations lie: Why many modified by attributions fail. In *Proceedings of the International Conference on Machine Learning (ICML)*, 2020.
- [24] Julius Adebayo, Justin Gilmer, Michael Muelly, Ian Goodfellow, Moritz Hardt, and Been Kim. Sanity checks for saliency maps. In *Advances in Neural Information Processing Systems (NIPS)*, 2018.
- [25] Dylan Slack, Anna Hilgard, Sameer Singh, and Himabindu Lakkaraju. Reliable post hoc explanations: Modeling uncertainty in explainability. *Advances in Neural Information Processing Systems (NeurIPS)*, 34, 2021.
- [26] Sukrut Rao, Moritz Böhle, and Bernt Schiele. Towards better understanding attribution methods. In *Proceedings of the IEEE Conference on Computer Vision and Pattern Recognition (CVPR)*, 2022.
- [27] Christian Szegedy, Wojciech Zaremba, Ilya Sutskever, Joan Bruna, Dumitru Erhan, Ian Goodfellow, and Rob Fergus. Intriguing properties of neural networks. *arXiv preprint arXiv:1312.6199*, 2013.
- [28] Aravindh Mahendran and Andrea Vedaldi. Understanding deep image representations by inverting them. In *Proceedings of the IEEE conference on computer vision and pattern recognition*, pages 5188–5196, 2015.
- [29] Anh Nguyen, Jason Yosinski, and Jeff Clune. Deep neural networks are easily fooled: High confidence predictions for unrecognizable images. In *Proceedings of the IEEE conference on computer vision and pattern recognition*, pages 427–436, 2015.
- [30] Mike Tyka. Class visualization with bilateral filters. 2016. URL: <https://mtyka.github.io/deepdream/2016/02/05/bilateral-class-vis.html>, 2(3).
- [31] M. Øygaard Audun. Visualizing googlenet classes. URL: <https://www.auduno.com/2015/07/29/visualizing-googlenet-classes/>, 2(3).
- [32] Dimitris Tsipras, Shibani Santurkar, Logan Engstrom, Alexander Turner, and Aleksander Madry. Robustness may be at odds with accuracy. *arXiv preprint arXiv:1805.12152*, 2018.
- [33] Shibani Santurkar, Andrew Ilyas, Dimitris Tsipras, Logan Engstrom, Brandon Tran, and Aleksander Madry. Image synthesis with a single (robust) classifier. *Advances in Neural Information Processing Systems*, 32, 2019.
- [34] Logan Engstrom, Andrew Ilyas, Shibani Santurkar, Dimitris Tsipras, Brandon Tran, and Aleksander Madry. Adversarial robustness as a prior for learned representations. *arXiv preprint arXiv:1906.00945*, 2019.
- [35] Alexander Mordvintsev, Christopher Olah, and Mike Tyka. Inceptionism: Going deeper into neural networks. 2015.
- [36] Donglai Wei, Bolei Zhou, Antonio Torralba, and William Freeman. Understanding intra-class knowledge inside cnn. *arXiv preprint arXiv:1507.02379*, 2015.
- [37] Anh Nguyen, Jason Yosinski, and Jeff Clune. Multifaceted feature visualization: Uncovering the different types of features learned by each neuron in deep neural networks. *Visualization for Deep Learning workshop, Proceedings of the International Conference on Machine Learning (ICML)*, 2016.
- [38] Anh Nguyen, Alexey Dosovitskiy, Jason Yosinski, Thomas Brox, and Jeff Clune. Synthesizing the preferred inputs for neurons in neural networks via deep generator networks. *Advances in neural information processing systems*, 29, 2016.
- [39] Anh Nguyen, Jeff Clune, Yoshua Bengio, Alexey Dosovitskiy, and Jason Yosinski. Plug & play generative networks: Conditional iterative generation of images in latent space. In *Proceedings of the IEEE conference on computer vision and pattern recognition*, pages 4467–4477, 2017.
- [40] Kaiming He, Xiangyu Zhang, Shaoqing Ren, and Jian Sun. Deep residual learning for image recognition. In *Proceedings of the IEEE Conference on Computer Vision and Pattern Recognition (CVPR)*, 2016.
- [41] A Dosovitskiy, L Beyer, Alexander Kolesnikov, Dirk Weissenborn, Xiaohua Zhai, Thomas Unterthiner, M Dehghani, Matthias Minderer, G Heigold, S Gelly, Jakob Uszkoreit, and N Houlsby. An image is worth 16x16 words: Transformers for image recognition at scale. *ICLR*, 2021.
- [42] Alan V Oppenheim and Jae S Lim. The importance of phase in signals. *Proceedings of the IEEE*, 69(5):529–541, 1981.
- [43] Terry Caelli and Paul Bevan. Visual sensitivity to two-dimensional spatial phase. *JOSA*, 72(10):1375–1381, 1982.
- [44] Nathalie Guyader, Alan Chauvin, Carole Peyrin, Jeanny Hérault, and Christian Marendaz. Image phase or amplitude? rapid scene categorization is an amplitude-based process. *Comptes Rendus Biologies*, 327(4):313–318, 2004.

- [45] Olivier R Joubert, Guillaume A Rousselet, Michele Fabre-Thorpe, and Denis Fize. Rapid visual categorization of natural scene contexts with equalized amplitude spectrum and increasing phase noise. *Journal of Vision*, 9(1):2–2, 2009.
- [46] Evgeny Gladilin and Roland Eils. On the role of spatial phase and phase correlation in vision, illusion, and cognition. *Frontiers in Computational Neuroscience*, 9:45, 2015.
- [47] Lucas Beyer, Pavel Izmailov, Alexander Kolesnikov, Mathilde Caron, Simon Kornblith, Xiaohua Zhai, Matthias Minderer, Michael Tschannen, Ibrahim Alabdulmohsin, and Filip Pavetic. Flexivit: One model for all patch sizes. *arXiv preprint arXiv:2212.08013*, 2022.
- [48] Thomas Fel, Agustin Picard, Louis Bethune, Thibaut Boissin, David Vigouroux, Julien Colin, Rémi Cadène, and Thomas Serre. Craft: Concept recursive activation factorization for explainability. *Proceedings of the IEEE Conference on Computer Vision and Pattern Recognition (CVPR)*, 2022.
- [49] Dumitru Erhan, Yoshua Bengio, Aaron Courville, and Pascal Vincent. Visualizing higher-layer features of a deep network. *University of Montreal*, 1341(3):1, 2009.
- [50] Guangrun Wang and Philip HS Torr. Traditional classification neural networks are good generators: They are competitive with ddpm’s and gans. *arXiv preprint arXiv:2211.14794*, 2022.
- [51] Alexander Mordvintsev, Nicola Pezzotti, Ludwig Schubert, and Chris Olah. Differentiable image parameterizations. *Distill*, 2018.
- [52] Judy Borowski, Roland S Zimmermann, Judith Schepers, Robert Geirhos, Thomas SA Wallis, Matthias Bethge, and Wieland Brendel. Exemplary natural images explain cnn activations better than state-of-the-art feature visualization. *arXiv preprint arXiv:2010.12606*, 2020.
- [53] Victor Boutin, Thomas Fel, Lakshya Singhal, Rishav Mukherji, Akash Nagaraj, Julien Colin, and Thomas Serre. Diffusion models as artists: Are we closing the gap between humans and machines? *arXiv preprint arXiv:2301.11722*, 2023.
- [54] Yiyu Sun, Yifei Ming, Xiaojin Zhu, and Yixuan Li. Out-of-distribution detection with deep nearest neighbors. In *International Conference on Machine Learning*, pages 20827–20840. PMLR, 2022.
- [55] Andrew G Howard, Menglong Zhu, Bo Chen, Dmitry Kalenichenko, Weijun Wang, Tobias Weyand, Marco Andreetto, and Hartwig Adam. Mobilenets: Efficient convolutional neural networks for mobile vision applications. *arXiv preprint arXiv:1704.04861*, 2017.
- [56] Karen Simonyan and Andrew Zisserman. Very deep convolutional networks for large-scale image recognition. *arXiv preprint arXiv:1409.1556*, 2014.
- [57] François Chollet. Xception: Deep learning with depthwise separable convolutions. In *Proceedings of the IEEE conference on computer vision and pattern recognition*, pages 1251–1258, 2017.
- [58] Mingxing Tan and Quoc Le. Efficientnet: Rethinking model scaling for convolutional neural networks. In *International conference on machine learning*, pages 6105–6114. PMLR, 2019.
- [59] Zhuang Liu, Hanzi Mao, Chao-Yuan Wu, Christoph Feichtenhofer, Trevor Darrell, and Saining Xie. A convnet for the 2020s. In *Proceedings of the IEEE/CVF Conference on Computer Vision and Pattern Recognition*, pages 11976–11986, 2022.
- [60] Gao Huang, Zhuang Liu, Laurens Van Der Maaten, and Kilian Q Weinberger. Densely connected convolutional networks. In *Proceedings of the IEEE conference on computer vision and pattern recognition*, pages 4700–4708, 2017.
- [61] Alexander Kolesnikov, Lucas Beyer, Xiaohua Zhai, Joan Puigcerver, Jessica Yung, Sylvain Gelly, and Neil Houlsby. Big transfer (bit): General visual representation learning. In *Computer Vision – ECCV 2020: 16th European Conference, Glasgow, UK, August 23–28, 2020, Proceedings, Part V*, page 491–507, Berlin, Heidelberg, 2020. Springer-Verlag.
- [62] Kaiming He, Xiangyu Zhang, Shaoqing Ren, and Jian Sun. Identity mappings in deep residual networks. In *Computer Vision–ECCV 2016: 14th European Conference, Amsterdam, The Netherlands, October 11–14, 2016, Proceedings, Part IV 14*, pages 630–645. Springer, 2016.
- [63] Timothy Dozat. Incorporating nesterov momentum into adam. 2016.
- [64] Thomas Fel, Lucas Hervier, David Vigouroux, Antonin Poche, Justin Plakoo, Remi Cadene, Mathieu Chalvidal, Julien Colin, Thibaut Boissin, Louis Bethune, Agustin Picard, Claire Nicodeme, Laurent Gardes, Gregory Flandin, and Thomas Serre. Xplique: A deep learning explainability toolbox. *Workshop on Explainable Artificial Intelligence for Computer Vision (CVPR)*, 2022.
- [65] Amirata Ghorbani, James Wexler, James Y Zou, and Been Kim. Towards automatic concept-based explanations. *Advances in Neural Information Processing Systems*, 32, 2019.
- [66] Robert Geirhos, Roland S. Zimmermann, Blair Bilodeau, Wieland Brendel, and Been Kim. Don’t trust your eyes: on the (un)reliability of feature visualizations, 2023.

- [67] Roland S Zimmermann, Judy Borowski, Robert Geirhos, Matthias Bethge, Thomas Wallis, and Wieland Brendel. How well do feature visualizations support causal understanding of cnn activations? *Advances in Neural Information Processing Systems*, 34:11730–11744, 2021.